

T1-weighted Dynamic Contrast-enhanced MRI to Differentiate Nonneoplastic and Malignant Vertebral Body Lesions in the Spine


Youxin Guan, BA • Kyung K. Peck, PhD • John Lyo, MD • Jamie Tisnado, MD • Eric Lis, MD • Julio Arevalo-Perez, MD • Yoshiya Yamada, MD • Meera R. Hameed, MD • Sasan Karimi, MD • Andrei Holodny, MD

From the Departments of Radiology (Y.G., K.K.P., J.L., J.T., E.L., J.A.P., S.K., A.H.), Medical Physics (K.K.P.), Radiation Oncology (Y.Y.), and Pathology (M.R.H.), Memorial Sloan-Kettering Cancer Center, 1275 York Ave, New York, NY 10021; Department of Radiology, Weill Medical College of Cornell University, New York, NY (A.H.); and Department of Neuroscience, Weill-Cornell Graduate School of the Medical Sciences, New York, NY (A.H.). Received March 14, 2019; revision requested May 17; revision received June 24, 2020; accepted July 2. Address correspondence to A.H. (e-mail: holodnya@mskcc.org).

Study supported by the National Cancer Institute of the National Institutes of Health (R25CA020449); supported in part by the National Institutes of Health/National Cancer Institute Cancer Center Support Grant (P30 CA008748). The content is solely the responsibility of the authors and does not necessarily represent the official views of the National Institutes of Health.

Conflicts of interest are listed at the end of this article.

See also the editorial by Haller in this issue.

Radiology 2020; 297:382–389 • <https://doi.org/10.1148/radiol.2020190553> • Content codes:  

Background: Dynamic contrast agent–enhanced (DCE) perfusion MRI may help differentiate between nonneoplastic and malignant lesions in the spine.

Purpose: To investigate the correlation between fractional plasma volume (V_p), a parameter derived from DCE perfusion MRI, and histopathologic diagnosis for spinal lesions.

Materials and Methods: In this retrospective study, patients who underwent DCE perfusion MRI and lesion biopsy between May 2015 and May 2018 were included. Inclusion criteria were short time interval (<30 days) between DCE perfusion MRI and biopsy, DCE perfusion MRI performed before biopsy, and DCE perfusion MRI performed at the same spine level as biopsy. Exclusion criteria were prior radiation treatment on vertebrae of interest, poor DCE perfusion MRI quality, nondiagnostic biopsy, and extensive spinal metastasis or prior kyphoplasty. One hundred thirty-four lesions were separated into a nonneoplastic group ($n = 51$) and a malignant group ($n = 83$) on the basis of histopathologic analysis. Two investigators manually defined regions of interest in the vertebrae. DCE perfusion MRI parameter V_p was calculated by using the Tofts pharmacokinetic two-compartment model. V_p was quantified, normalized to adjacent normal vertebrae, and compared between the two groups. A Mann-Whitney U test and receiver operating characteristic analysis was performed to verify the difference in V_p between the nonneoplastic and malignant groups. Reproducibility was assessed by calculating the Cohen κ coefficient.

Results: One hundred patients (mean age, 65 years \pm 11 [standard deviation]; 52 men) were evaluated. V_p was lower in nonneoplastic lesions versus malignant lesions (1.6 ± 1.3 vs 4.2 ± 3.0 , respectively; $P < .001$). The sensitivity of V_p was 93% (77 of 83; 95% confidence interval [CI]: 85%, 97%), specificity was 78% (40 of 51; 95% CI: 65%, 89%), and area under the receiver operating characteristic curve was 0.88 (95% CI: 0.82, 0.95). Cohen κ coefficient suggested substantial agreement in both intra- ($\kappa = 0.72$) and interreader ($\kappa = 0.70$) reproducibility.

Conclusion: This study indicated that dynamic contrast agent–enhanced perfusion MRI parameter, fractional plasma volume, was able to differentiate between nonneoplastic spinal lesions and malignant lesions.

© RSNA, 2020

Online supplemental material is available for this article.

Cancer is a global burden and it is estimated that 12.7 million new cases worldwide in 2008 will increase to 22.2 million by 2030 (1). Among patients with cancer, the skeletal system is the third most common metastatic site after the liver and the lungs, and the spine is the most common site of bone metastases (2–4). Metastatic disease to the spine can weaken the vertebrae with pathologic fractures, causing pain and deterioration in quality of life (5). In addition to creating mechanical instability, metastatic spinal lesions also precipitate neurologic complications because of spinal cord and nerve root compression (6).

MRI is the imaging modality of choice in detecting and evaluating spinal tumors. However, conventional MRI is sometimes unable to help differentiate between metastases

and benign vertebral body lesions in patients with cancer (7). Conventional MRI has been shown to be limited in complex cases where nonneoplastic bone disease such as osteoporosis resulting from cancer treatment and/or aging can present diagnostic challenges (8). In such indeterminate cases, biopsy is often necessary, and MRI can be used to locate lesions suspicious for cancer metastases and to guide treatment planning.

Previous studies have shown that dynamic contrast agent–enhanced (DCE) perfusion MRI may add valuable information for diagnosing cancer and evaluating treatment response, as the perfusion parameters, especially fractional plasma volume (V_p), a measure of tumor vascularity in the intravascular compartment, change at exposure to radiation

Abbreviations

CI = confidence interval, DCE = dynamic contrast enhanced, ROI = region of interest, V_p = fractional plasma volume

Summary

Nonneoplastic lesions and malignant lesions in the spine showed a difference in fractional plasma volume at dynamic perfusion MRI, which may improve accuracy for assessment of spinal malignancy.

Key Results

- The fractional plasma volume in the spine lesion compared with that of normal bone was greater in malignant lesions versus non-malignant lesions (4.2 vs 1.6; $P < .001$).
- Dynamic contrast agent-enhanced perfusion MRI had a sensitivity of 93% and specificity of 78% in differentiating between non-neoplastic and malignant vertebral body lesions in patients with malignancy.

therapy (9–11). The noninvasive nature of DCE perfusion MRI is less burdensome than biopsy to patients with cancer who need close monitoring over time for evaluation of disease progression and response to therapy.

The objective of this study was to investigate the correlation between V_p , a parameter derived from DCE perfusion MRI, and histopathologic diagnosis for spinal lesions. We hypothesized that V_p would be different between nonneoplastic lesions and metastases.

Materials and Methods

We conducted this retrospective study with a waiver of authorization from the institutional review board for patient consent. The study was conducted in a Health Insurance Portability and Accountability Act-compliant manner.

Study Patients

We searched our institutional radiology database for patients who underwent DCE perfusion MRI and underwent a biopsy of the lesion of interest between May 2015 and May 2018 (Fig 1). Inclusion criteria were short interval (<30 days) between DCE perfusion MRI and biopsy to allow for accurate representation of the perfusion status on the biopsied lesion, DCE perfusion MRI performed before biopsy to avoid the effect of biopsy-related changes on DCE parameters, and DCE perfusion MRI performed at the spine level where biopsy was performed. All biopsy results were reviewed by a pathologist and deemed to be of diagnostic quality. Exclusion criteria were previous radiation treatment in the vertebrae of interest, poor DCE perfusion MRI quality, nondiagnostic biopsy, and extensive spinal metastasis or prior kyphoplasty.

MRI Acquisition

We performed MRI of the spine with a 1.5-T scanner (GE Healthcare, Milwaukee, Wis) by using an eight-channel cervical-thoracic-lumbar surface coil. All patients underwent routine MRI sequences: sagittal T1 (field of view, 32–36 cm; slice thickness, 3 mm; repetition time, 400–650 msec; and flip angle, 90°), sagittal T2 (field of view, 32–36 cm; slice thickness, 3 mm; repetition time, 3500–4000 msec; and flip angle, 90°), and sagittal short τ inversion recovery (field of view, 32–36 cm; slice thickness, 3 mm; repetition time, 3500–6000 msec; and flip angle, 90°).

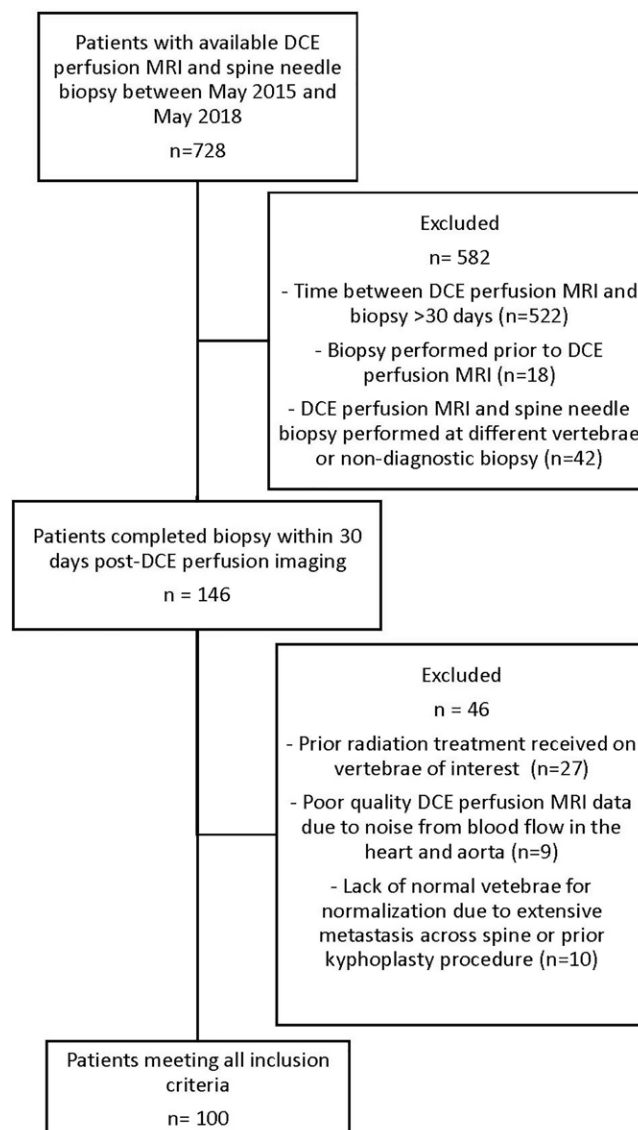


Figure 1: Inclusion and exclusion criteria of patients with spinal lesions undergoing dynamic contrast agent-enhanced (DCE) perfusion MRI and biopsy.

A DCE perfusion MRI in the spine was then performed. Gadobutrol (Bayer, Barmen, Germany) was administered at 0.1 mmol/kg body weight and a rate of 2–3 mL/sec. Kinetic enhancement of the tissue during and after injection of gadopentetate dimeglumine was obtained by using a three-dimensional T1-weighted fast spoiled-gradient echo sequence (repetition time msec/echo time msec, 4–5/1–2; slice thickness, 5 mm; flip angle, 25°; field of view, 32 cm; and temporal resolution, 5–6 seconds) and consisted of 10–12 images in the sagittal plane. The three-dimensional spoiled-gradient sequences generated phase images in addition to the standard magnitude images. The duration of the DCE sequence was 300 seconds. Sagittal and axial T1-weighted gadopentetate dimeglumine-enhanced MRI scans were acquired after DCE perfusion MRI.

Biopsy Sampling and Pathology

All patients underwent CT-guided spine biopsies by using a CT scanner (1200SX; Picker International, Cleveland, Ohio) under

moderate sedation. The previously established institutional guidelines were followed (12). Briefly, 2.5×2.5 -mm axial images were obtained through the target lesion vertebrae. Typically, a coaxial technique was used with the biopsy needle trajectory determined by anatomy and lesion location. Core biopsy was obtained by using 11-gauge or 13-gauge needles (Madison Perforating Bone Biopsy System; Merit Medical Systems, South Jordan, Utah) in all patients. During the biopsy procedure, a cytology technologist reviewed touch preparations from core biopsies to ensure specimen adequacy. Only patients who met the following criteria were included in the nonneoplastic category, as follows: (a) Definite diagnosis on biopsy. These included acute inflammation, osteoporosis, fragments of bone with changes of remodeling consistent with fracture, necrosis likely secondary to treatment-related changes; and (b) in those lesions where the diagnosis was nonspecific (for example, no evidence of malignancy), we only included those who were stable at CT or MRI for at least 6 months.

Data Analysis

Data were blinded, processed, and analyzed by a single trained researcher (Y.G.) and a senior neuroradiologist (A.H.) independently by using a U.S. Food and Drug Administration–approved commercial software (NordicIce, version 2.3; NordicNeuroLab, Milwaukee, Wis). Preprocessing steps included background noise removal, spatial and temporal smoothing, and automatic detection of the arterial input function from the aorta. Arterial input function was individually computed and visually verified in every slice, and arterial input function curves with a rapid increase in signal enhancement and sharp peak followed by minimal temporal noises were selected for further DCE analysis.

We applied the extended Tofts two-compartment pharmacokinetic model (13), which assumes that the contrast agent is either in the interstitial space or in the intravascular compartment, to calculate the DCE perfusion MRI parameter V_p . Regions of interest (ROIs) were manually defined around the spinal lesions with careful considerations to exclude venous structures, hemangiomas, disc spaces, cortical bone, and spondylotic changes on each T1-weighted DCE perfusion MRI slice. Structures of interest include vertebral body, lamina, spinous process, and paraspinal soft tissues. ROIs were then superimposed onto corresponding perfusion maps to guide ROI calculations. When the lesions appeared to extend beyond osseous structure into paraspinal soft tissues, we included both the bony and soft structures in our ROI analysis. In cases where the lesion spanned multiple MRI slices, ROI values from each slice were averaged to yield the final parameter value.

Measurements on all lesions were performed by two investigators independently: (a) a research fellow (Y.G.) with one of two senior neuroradiologists (S.K. and J.L.) approving every case, and (b) a senior neuroradiologist (A.H., with 25 years of experience). To test for intraobserver variability, measurements in a were repeated in all of the lesions by the same reader (Y.G.) at a different time by using the same method to collect a second set of interpretations for intrareproducibility analysis. To test for interobserver variability, the measurements in a and b were compared. To account for the background variations among different DCE perfusion MRI studies, we normalized fractional plasma volume by obtaining the ratio between the lesion ROI and its neighboring healthy vertebra

Table 1: Patient Demographics

Parameter	Total	Nonneoplastic	Malignant
No. of lesions	134	51	83
Mean age (y)	66 ± 11	64 ± 11	65 ± 11
Sex			
No. of men	52	11	41
No. of women	48	19	26
Site of spinal lesion			
Cervical	2	2	0
Thoracic	60	22	38
Lumbar	66	25	41
Sacral	6	2	4

Note.—Mean data are \pm standard deviation. Some patients had multiple biopsied spinal lesions, which were counted as separate lesions since the lesions were biopsied and studied independently. Among all the patients, 75 patients had one biopsied lesion, 18 patients had two biopsied lesions, five patients had three biopsied lesions, and two patients had four biopsied lesions.

Table 2: Lesion by Primary Cancer Type

Parameter	All Lesions	Nonneoplastic Lesions	Malignant Lesions*
Total primary cancers	134	51	83
Solid tumor			
Lung	32	16	16
Breast	16	3	13
Kidney	8	1	7
Prostate	8	0	8
Colon	7	3	4
Ovarian	5	5	0
Bladder	4	1	3
Skin	4	0	4
Sarcoma	4	2	2
Thyroid	4	2	2
Other	15	5	10
Total	107	38	69
Hematologic malignancy			
Multiple myeloma	16	4	12
Lymphoma	4	2	2
Other	4	4	0
Total	24	10	14
No cancer	3	3	0

* Lesions in the malignant category were metastases from patient's primary cancer.

(ie, V_p normalization = V_p of lesion ROI/ V_p of normal bone). The normalized V_p values were then used for statistical analyses.

Statistical Analysis

We performed a Mann-Whitney U test wherein P values of .05 or less indicated statistical significance on V_p to evaluate if it was significantly different between the nonneoplastic group and malignant group. We treated multiple lesions in the same patient as independent lesions because they were individually biopsied and

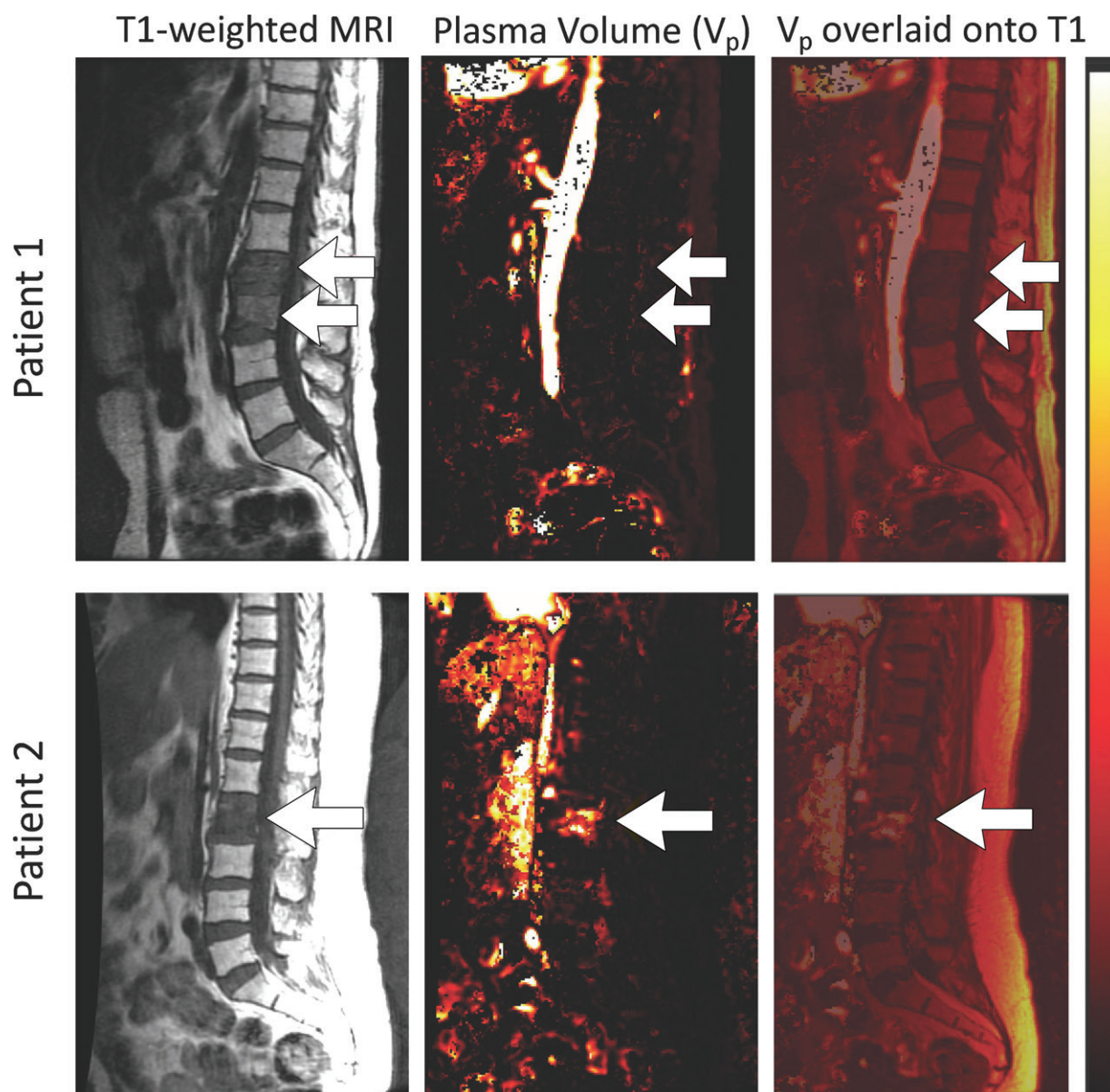


Figure 2: Example of two patients with colon cancer. The left column shows sagittal T1-weighted MRI of the lower spine. Hypointense regions indicate vertebral lesions. Arrows point to biopsy-verified vertebrae of interest. In the top row, patient 1 had biopsied spinal lesion reported by pathology as no evidence of malignancy at L2–3 (left column). In the bottom row, patient 2 had malignant lesions at L2. The middle column shows fractional plasma volume (V_p) maps of the lesions. Increased signal intensity was observed in malignant lesions. The V_p for patient 1 was 0.9, for patient 2 the V_p was 5.8. The right column shows merged T1-weighted MRI and dynamic contrast agent-enhanced perfusion MRI V_p map.

studied during the analysis. We performed receiver operating characteristic analysis by using software (SPSS v26 GradPacks; IBM, Armonk, NY) to determine the optimal cutoff with the highest Youden index. Cohen κ coefficient was calculated to assess reproducibility by analyzing the extent of agreement within measurements by the same reader (Y.G.) and between measurements by two different readers (Y.G. and A.H.).

Results

Study Patients

A total of 100 patients met inclusion criteria (Table 1), composed of 52 men and 48 women with similar age distribution. The mean age for all patients was 65 years \pm 11 (standard deviation). Among

all patients, 30 patients had nonneoplastic lesions, 67 patients had malignant lesions, and three patients had both. Among all patients, 75 patients had one biopsied lesion, 18 patients had two biopsied lesions, five patients had three biopsied lesions, and two patients had four biopsied lesions. A list of nonneoplastic lesions is provided in Table E1 (online).

As shown in Table 2, the cohort represented a heterogeneous group of primary cancers. A total of 134 spinal lesions involving the cervical to sacral spine were analyzed. According to histopathologic analysis, 51 of 134 (38.0%) lesions were nonneoplastic, whereas the remaining 83 (61.9%) lesions were malignant. The three most frequently seen primary cancers were lung (24.0%; 32 of 134), breast (11.9%; 16 of 134), and multiple myeloma (11.9%; 16 of 134).

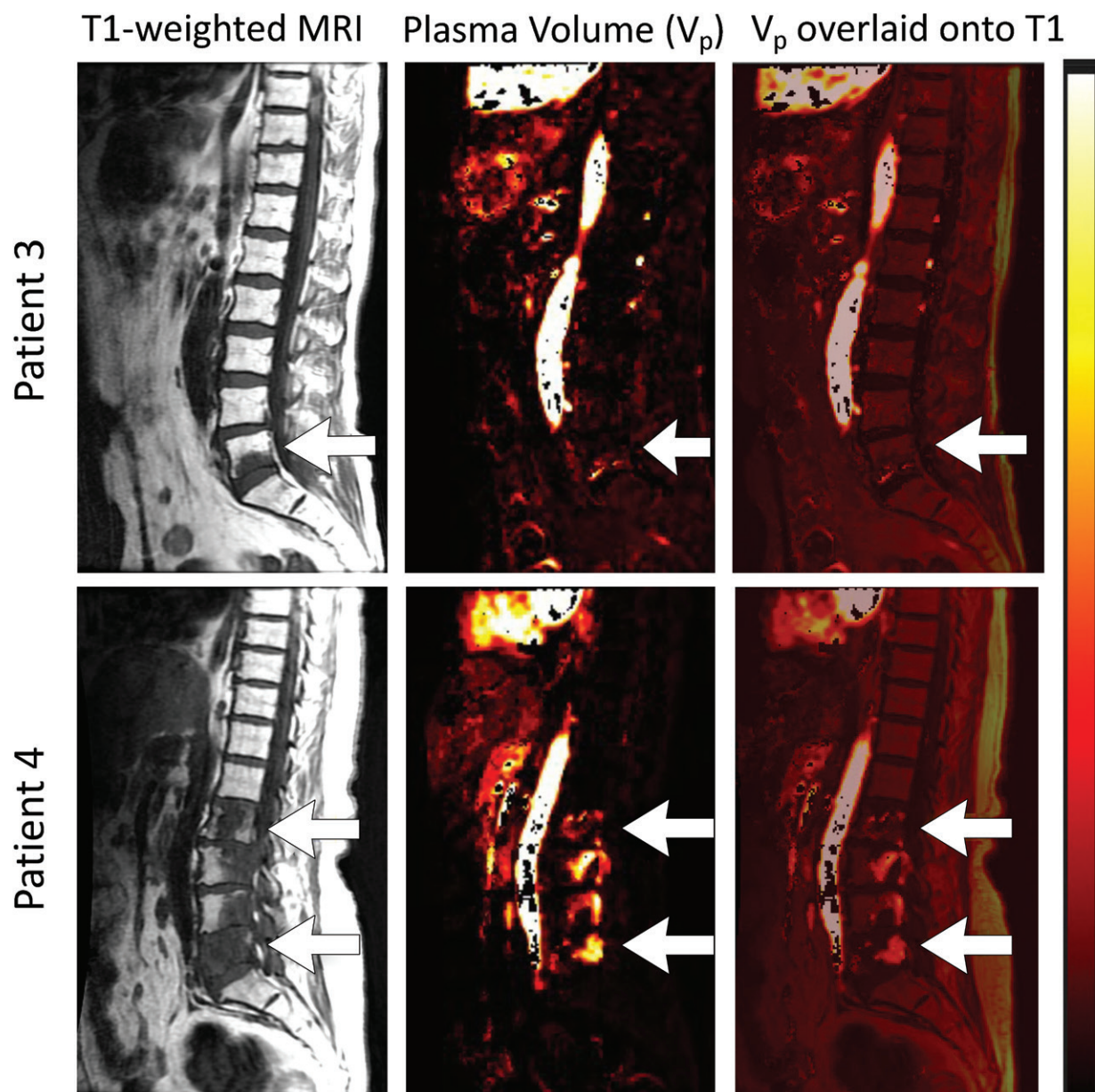


Figure 3: Example of two patients with bladder cancer. In the top row, patient 3 had spinal lesion of bone fragments with marrow fibrosis at L5 (left; arrows). Fractional plasma volume (V_p) maps (middle) and merged T1-weighted MRI and dynamic contrast agent-enhanced perfusion MRI V_p maps (right) of the lesions are shown. In the bottom row, patient 4 had malignant lesions at L2–5 (arrows). The V_p for patient 3 was 1.4, for patient 4 the V_p was 12.2 (L2, L5 averaged).

Analysis of Tumor Perfusion at DCE MRI

On T1-weighted images from MRI, all lesions appeared hypointense. On the V_p maps, however, only the malignant lesions displayed increased signal intensity, whereas the nonneoplastic lesions showed minimal to no signal increase and looked similar to the other vertebra (Figs 2, 3).

As shown in Figure 4, the mean V_p for nonneoplastic lesions was 1.6, and the mean V_p for malignant lesions was 4.2. There was little overlap in V_p between nonneoplastic lesions and malignant lesions as suggested by the fact that the first quartile of the V_p for malignant lesions was 2.2, whereas the third quartile of the V_p for nonneoplastic lesions was 1.5. Lesions that originated from both solid tumors and hematologic malignancies showed a

similar V_p distribution. The Mann-Whitney U test verified that the difference between the V_p in the nonneoplastic group and malignant group was significant ($P < .001$).

Among 134 lesions, 11 had elevated V_p above the cutoff value of 1.6 despite having a nonneoplastic histopathologic result (samples 41–51 in Table E1 [online]), whereas six biopsy-proven malignant lesions had V_p below the cutoff. Figure 5 illustrates representative examples of such lesions with false-positive and false-negative findings.

By using an optimal V_p cutoff of 1.6 as suggested by receiver operating characteristic analysis (area under the receiver operating characteristic curve, 0.88; 95% confidence interval [CI]: 0.82, 0.95) (Table 3) and a maximal Youden index at 0.71, V_p

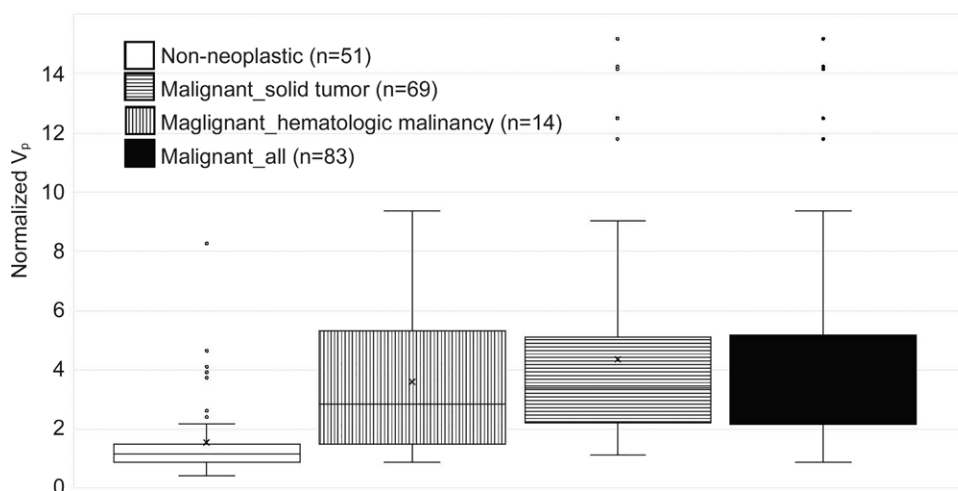


Figure 4: Box and whisker plot of fractional plasma volume (V_p) by group. The average V_p in the nonneoplastic group (non-neoplastic) was 1.6 ± 1.3 , and the average V_p in the malignant group (malignant_all) was 4.2 ± 3.0 . Lesions originating from hematologic malignancies (malignant_hematologic malignancy) and from solid tumors (malignant_solid tumor) showed a similar distribution of V_p , with an average of 3.6 ± 2.5 and 4.3 ± 3.1 , respectively. There was a difference in V_p between the nonneoplastic group and malignant group as evidenced by a Mann-Whitney U test ($P < .001$).

had a sensitivity of 93% (77 of 83; 95% CI: 85%, 97%) and specificity of 78% (40 of 51; 95% CI: 65%, 89%) when DCE perfusion MRI was used to differentiate nonneoplastic and malignant lesions (Fig 6). The Cohen κ coefficient calculated from intrareproducibility analysis was 0.72, whereas the Cohen κ coefficient calculated from interreproducibility analysis was 0.70.

Discussion

Previous studies emphasized the use of dynamic contrast agent-enhanced (DCE) perfusion MRI in evaluating spinal lesions (9–11,14–16). These studies were conducted in small selective patient populations and suggested the perfusion parameter fractional plasma volume (V_p), derived from DCE perfusion MRI, can detect viable tumor in the spine. Expanding from these precedent studies, the goal of this study was to investigate the correlation between DCE perfusion MRI parameters and histopathologic diagnosis in the general cancer patient population. Our results showed a significant difference in V_p between the nonneoplastic lesions and malignant lesions (1.6 ± 1.3 vs 4.2 ± 3.0 , respectively; $P < .001$) with a sensitivity of 93% (95% confidence interval [CI]: 85%, 97%) and specificity of 78% (95% [CI]: 65%, 89%), demonstrating that the perfusion parameter V_p is able to differentiate between malignant and nonneoplastic spinal lesions in a wide range of primary cancers, including hypovascular cancers such as breast cancer and prostate cancer.

Prior studies described the utility of DCE perfusion in vertebral metastases. Chu et al (9), Kumar et al (10), and Lis et al (11) described the precipitous drop in V_p changes in spinal metastases at different times after radiation therapy. Arevalo-Perez et al (14) and Saha et al (15) described the ability of DCE perfusion MRI to help differentiate between benign and malignant spinal fractures and hyper- and hypovascular spinal metastases, respectively. Morales et al (16) used V_p to differentiate atypical hemangiomas, the most common benign tumors in spine, from vertebral metastatic lesions. In our study, we observed that V_p changes occurred in spinal metastases from a wide variety of primary cancers. The

increased V_p in spinal metastases is probably because of increased tumor neovascularity. Tumors acquire increased blood supply from multiple mechanisms (17). The abnormal vascular network within a metastatic lesion allows for the contrast agent to accumulate within the tumor vascular network, resulting in an increased V_p on the DCE perfusion MRI scan.

We observed that the perfusion signal was not limited to the bony structure of the spine but could also be detected in the epidural space and surrounding soft tissues. DCE perfusion MRI was able to help detect increased tumor vascularity in the paraspinal muscles and spinal

canal, allowing for the assessment of tumor spread beyond the skeletal system.

V_p was elevated in some cases of benign vertebral fractures, contributing to all 11 lesions with false-positive findings. This phenomenon may be attributed to natural responses to recent injury where healing processes including inflammation and angiogenesis take place (18). For example, several patients had suspected osteoporotic fractures, which were confirmed to be benign at biopsy, despite increased perfusion parameters associated with the fractures. In addition, some malignant lesions (six of 83) had low contrast agent uptake, resulting in a false-negative V_p value even though biopsy samples showed evidence of malignancy. The reason for lack of contrast agent uptake in these lesions was unclear, possibly because of the limited tumor vasculatures that developed within these metastases.

At DCE perfusion MRI data analysis, ROI placements were put in the signal enhancement region of the V_p map. On the basis of our experience, slightly displaced location of ROIs does not result in significant change of the calculated average V_p value. As suggested by the Cohen κ coefficient obtained in this study, there is substantial agreement between repeat measurements within the same reader ($\kappa = 0.72$; substantial agreement range, 0.61–0.80) and between two independent readers ($\kappa = 0.70$), suggesting a strong reproducibility in the DCE data.

Our study had limitations. Sensitivity and specificity measurements obtained in this study were on the basis of a single institution, a single scanner manufacturer, and a single method of analysis. These will need to be confirmed by other institutions with other scanner manufacturers and methods of DCE analysis to optimize the estimation of sensitivity and specificity, and the V_p cutoff. Last, there are three patients in whom both nonneoplastic and malignant lesions were manifest. Because of the small sample size, cluster effect and lesion level analysis were not performed in this study.

Although DCE perfusion MRI has been described to increase the sensitivity and specificity of routine conventional imaging of

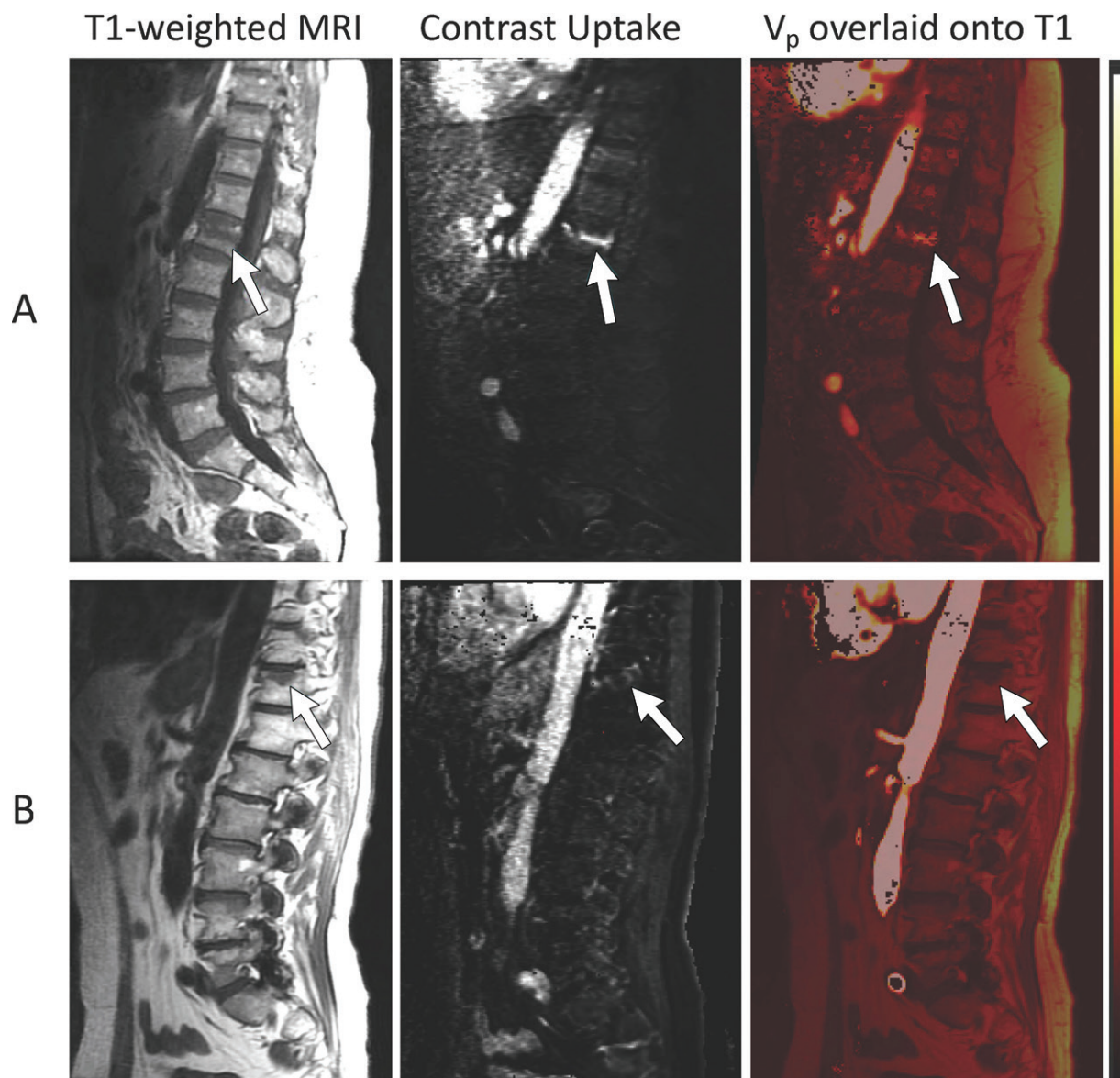


Figure 5: Examples of lesions with false-positive and false-negative findings. A, Images in a 62-year-old female patient with primary pancreatic neuroendocrine cancer and the following spine biopsy pathology report: "Bone marrow with trilineage hematopoiesis. No tumor seen. Negative pan-cytokeratin." The nonneoplastic lesion at L1 had increased contrast uptake (middle column) with a V_p of 3.7 (right column). B, Images in a 69-year-old male patient with metastatic esophageal cancer at T11 with the following spine biopsy pathology report: "Metastatic poorly differentiated carcinoma, consistent with esophageal primary." The malignant lesion had limited contrast uptake (middle column) with a V_p of 1.1 (right column). The arrows point to biopsy-verified vertebrae of interest.

the spine for early detection of treatment response and failure (9,10), competing demands for high-spatial resolution, acquisition coverage, and signal-to-noise result in inadequate temporal resolution for accurate measurement of the arterial input function. Low sampling rate because of low temporal resolution can affect the time course of arterial input function and initial contrast agent wash-in. Furthermore, DCE perfusion MRI is currently performed only in the sagittal plane because of the consideration of imaging time and coverage. The restricted angle also limits its ability to depict lesions that are better seen on the axial plane. Because of the lack of established method to quantify the diagnostic value of conventional MRI, an analysis on the diagnostic performance of conventional MRI was not performed in our study. Future studies are necessary to investigate

the diagnostic value obtained from a combined method from conventional MRI and DCE perfusion MRI.

Diffusion-weighted imaging is another widely used MRI sequence that can help differentiate between nonneoplastic and malignant lesions (19,20). For example, Xing et al (19) used math models of DWI to differentiate metastases and myeloma with receiver operating characteristic curves in the range of 0.7. Lee et al (20) differentiated Schmorl nodes from metastases with a receiver operating characteristic of 0.94. As one of the limitations, data from diffusion-weighted imaging were not available for analysis in our retrospective study because it is not part of the standard clinical protocol for the spine at our institution.

In conclusion, our results indicated that the dynamic contrast agent-enhanced (DCE) perfusion MRI parameter, fractional

Table 3: Proportions and Area Under the Receiver Operating Characteristic Curve

Parameter	Positive at Pathology	Negative at Pathology	Total
V_p positive ≥ 1.6	77	11	88
V_p negative < 1.6	6	40	46
Total	83	51	134
AUC	0.88 (0.82, 0.95)		

Note.—Data in parentheses are asymptotic 95% confidence intervals. AUC = area under curve, V_p = fractional plasma volume.

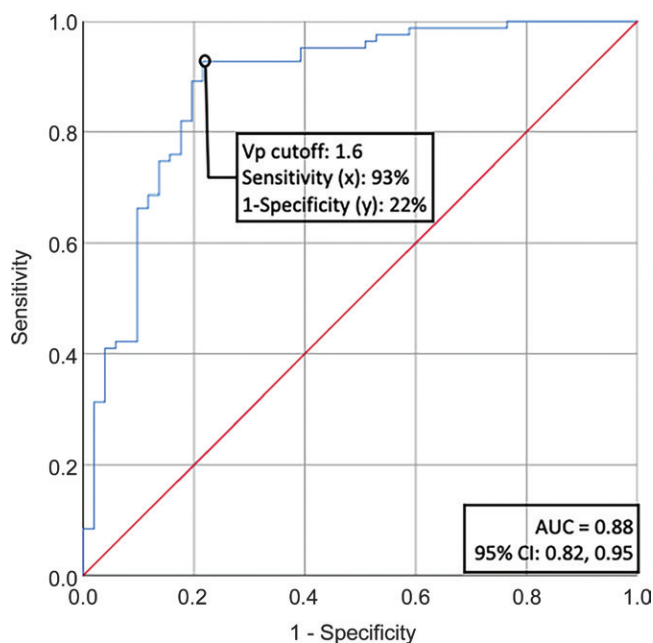


Figure 6: Receiver operating characteristic curve of the fractional plasma volume (V_p ; area under the receiver curve, 0.88; 95% confidence interval [CI]: 0.82, 0.95). The optimal V_p cutoff was calculated at 1.6, which yielded a sensitivity of 93% (77 of 83; 95% CI: 85%, 97%) and a specificity of 78% (40 of 51; 95% CI: 65%, 89%) by using dynamic contrast agent-enhanced MRI perfusion imaging data.

plasma volume, is able to differentiate between nonneoplastic spinal lesions and malignant lesions. Future directions of DCE perfusion MRI research include evaluating its effectiveness in predicting treatment response and comparing the diagnostic performance among conventional MRI, DCE perfusion MRI, and both combined.

Acknowledgment: We thank Joanne Chin, MFA, ELS, for her professional editorial assistance in the writing of this manuscript.

Author contributions: Guarantors of integrity of entire study, Y.G., K.K.P., J.L., S.K.; study concepts/study design or data acquisition or data analysis/interpretation, all authors; manuscript drafting or manuscript revision for important intellectual content, all authors; approval of final version of submitted manuscript, all authors; agrees to ensure any questions related to the work are appropriately resolved, all authors; literature research, Y.G., K.K.P., J.L., J.T., E.L., J.A.P.; clinical studies, Y.G., K.K.P., J.L., E.L., J.A.P., Y.Y., S.K., A.H.; experimental studies, K.K.P., Y.Y.; statistical analysis, Y.G.; and manuscript editing, all authors.

Disclosures of Conflicts of Interest: Y.G. disclosed no relevant relationships. K.K.P. disclosed no relevant relationships. J.L. disclosed no relevant relationships. J.T. disclosed no relevant relationships. E.L. Activities related to the present article: disclosed no relevant relationships. Activities not related to the present article: disclosed money paid to author for lectures from Medtronic; disclosed money paid to author for educational presentations from Medtronic. Other relationships: disclosed no relevant relationships. J.A.P. disclosed no relevant relationships. Y.Y. Activities related to the present article: disclosed no relevant relationships. Activities not related to the present article: disclosed money paid to author for consultancy from University of Wollongong; disclosed volunteer consultancy from Chordoma Foundation; disclosed payment for lectures from BrainLab and Vision RT. Other relationships: disclosed no relevant relationships. M.R.H. disclosed no relevant relationships. S.K. disclosed no relevant relationships. A.H. Activities related to the present article: disclosed no relevant relationships. Activities not related to the present article: disclosed no relevant relationships. Other relationships: disclosed money paid to author from fMRI Consultants.

References

- Bray F, Jemal A, Grey N, Ferlay J, Forman D. Global cancer transitions according to the Human Development Index (2008-2030): a population-based study. *Lancet Oncol* 2012;13(8):790-801.
- Roodman GD. Mechanisms of bone metastasis. *N Engl J Med* 2004;350(16):1655-1664.
- Mundy GR. Metastasis to bone: causes, consequences and therapeutic opportunities. *Nat Rev Cancer* 2002;2(8):584-593.
- Togawa D, Lewandrowski K-U. The pathophysiology of spinal metastases. In: McLain RF, Lewandrowski KU, Markman M, et al, eds. *Cancer in the Spine*. Totowa, NJ: Humana, 2006; 17-23.
- Chow E, Harris K, Fan G, Tsao M, Sze WM. Palliative radiotherapy trials for bone metastases: a systematic review. *J Clin Oncol* 2007;25(11):1423-1436.
- Byrne TN. Spinal cord compression from epidural metastases. *N Engl J Med* 1992;327(9):614-619.
- Norman D, Mills CM, Brant-Zawadzki M, Yeates A, Crooks LE, Kaufman L. Magnetic resonance imaging of the spinal cord and canal: potentials and limitations. *AJR Am J Roentgenol* 1983;141(6):1147-1152.
- Coleman R, Body JJ, Aapro M, Hadji P, Herrstedt J; ESMO Guidelines Working Group. Bone health in cancer patients: ESMO Clinical Practice Guidelines. *Ann Oncol* 2014;25(Suppl 3):iii124-iii137.
- Chu S, Karimi S, Peck KK, et al. Measurement of blood perfusion in spinal metastases with dynamic contrast-enhanced magnetic resonance imaging: evaluation of tumor response to radiation therapy. *Spine* 2013;38(22):E1418-E1424.
- Kumar KA, Peck KK, Karimi S, et al. A Pilot Study Evaluating the Use of Dynamic Contrast-Enhanced Perfusion MRI to Predict Local Recurrence After Radiosurgery on Spinal Metastases. *Technol Cancer Res Treat* 2017;16(6):857-865.
- Lis E, Saha A, Peck KK, et al. Dynamic contrast-enhanced magnetic resonance imaging of osseous spine metastasis before and 1 hour after high-dose image-guided radiation therapy. *Neurosurg Focus* 2017;42(1):E9.
- Lis E, Bilsky MH, Pisinski L, et al. Percutaneous CT-guided biopsy of osseous lesion of the spine in patients with known or suspected malignancy. *AJNR Am J Neuroradiol* 2004;25(9):1583-1588.
- Tofts PS, Brix G, Buckley DL, et al. Estimating kinetic parameters from dynamic contrast-enhanced T(1)-weighted MRI of a diffusible tracer: standardized quantities and symbols. *J Magn Reson Imaging* 1999;10(3):223-232.
- Arevalo-Perez J, Peck KK, Lyo JK, Holodny AI, Lis E, Karimi S. Differentiating benign from malignant vertebral fractures using T1-weighted dynamic contrast-enhanced MRI. *J Magn Reson Imaging* 2015;42(4):1039-1047.
- Saha A, Peck KK, Lis E, Holodny AI, Yamada Y, Karimi S. Magnetic resonance perfusion characteristics of hypervascular renal and hypovascular prostate spinal metastases: clinical utilities and implications. *Spine* 2014;39(24):E1433-E1440.
- Morales KA, Arevalo-Perez J, Peck KK, Holodny AI, Lis E, Karimi S. Differentiating Atypical Hemangiomas and Metastatic Vertebral Lesions: The Role of T1-Weighted Dynamic Contrast-Enhanced MRI. *AJNR Am J Neuroradiol* 2018;39(5):968-973.
- Carmeliet P, Jain RK. Molecular mechanisms and clinical applications of angiogenesis. *Nature* 2011;473(7347):298-307.
- Loi F, Córdova LA, Pajarinen J, Lin TH, Yao Z, Goodman SB. Inflammation, fracture and bone repair. *Bone* 2016;86:119-130.
- Xing X, Zhang J, Chen Y, Zhao Q, Lang N, Yuan H. Application of monoexponential, biexponential, and stretched-exponential models of diffusion-weighted magnetic resonance imaging in the differential diagnosis of metastases and myeloma in the spine: Univariate and multivariate analysis of related parameters. *Br J Radiol* 2020. 10.1259/bjr.20190891. Published online June 11, 2020.
- Lee JH, Park S. Differentiation of Schmorl Nodes From Bone Metastases of the Spine: Use of Apparent Diffusion Coefficient Derived From DWI and Fat Fraction Derived From a Dixon Sequence. *AJR Am J Roentgenol* 2019;213(5):W228-W235.